www.czasopisma.pan.pl PAN POLSKA AKADEMIA NAUK www.journals.pan.pl

PAN ARCHIVES OF ACOUSTICS
Vol. **45**, No. 4, pp. 647–654 (2020)
DOI: 10.24425/aoa.2020.135252

Research Paper

Selected Aspects of Meshless Method Optimization in the Room Acoustics with Impedance Boundary Conditions

Edyta PRĘDKA*, Anna KOCAN-KRAWCZYK, Adam BRAŃSKI

Department of Electrical and Computer Engineering Fundamentals
Faculty of Electrical and Computer Engineering, Technical University of Rzeszow
Rzeszow, Poland
*Corresponding Author e-mail: edytap@prz.rzeszow.pl

(*received June 2, 2020; accepted July 23, 2020*)

Two optimization aspects of the meshless method (MLM) based on nonsingular radial basis functions (RBFs) are considered in an acoustic indoor problem. The former is based on the minimization of the mean value of the relative error of the solution in the domain. The letter is based on the minimization of the relative error of the solution at the selected points in the domain. In both cases the optimization leads to the finding relations between physical parameters and the approximate solution parameters. The room acoustic field with uniform, impedance walls is considered.

As results, the most effective Hardy's Radial Basis Function (H-RBF) is pointed out and the number of elements in the series solution as a function of frequency is indicated. Next, for H-RBF and fixed n, distributions of appropriate acoustic fields in the domain are compared. It is shown that both aspects of optimization improve the description of the acoustic field in the domain in a strictly defined sense.

Keywords: architectural acoustics; meshless method; radial basis functions; impedance boundary condition.

1. Introduction

The main purpose of room acoustics is to describe the steady state of enclosed spaces. There are many methods for exact and numerical modelling of the interior acoustic field. Up to now the most popular numerical techniques draw on mesh-based methods such as the Finite Element Method (FEM), Boundary Element Method (BEM), Finite Differences Method (FDM), Trefftz Method (TM), Meshless Method (MLM) and many hybrid methods. All of them belong to the wave-based methods (WBM), (Prędka, Brański, 2020, and references cited therein). Heuristic methods are also important. They include acoustic image source methods (ISM) based on the geometric diffraction theory and acoustic energy methods (AEM) based on the principle of energy conservation. All of the above-mentioned methods have advantages and disadvantages. In order to remove or alleviate disadvantages, these methods are modified. In addition, hybrid methods are created for the same purpose.

And so in (Meissner, 2019) an exact (modal representation) of a room impulse response was used to describe acoustic field for low-frequency in rooms of arbitrary shape and walls covered by a material of complex impedance. In (Shi *et al.*, 2019) an exact (3D modified Fourier method) was applied to the description of the acoustic field of coupled rooms. In this case the solution series was supplemented with auxiliary functions, which were introduced to ensure the uniform convergence of the solution over the entire solution domain. In (Meissner, Wiśniewski, 2019) an exact method (modal expansion) was applied to study the impact of room modes on low-frequency transients. The sound source was a tone burst. A theoretical analysis was confirmed by FEM for two coupled rooms. In (Van Horssen *et al.*, 2018) applying characteristic coordinates, an exact solution (formula of d'Alembert), was achieved for initial-boundary problem described by the wave equation and Robin boundary conditions. In the work (Chen *et al.*, 2019) the BEM, based on non-uniform rational B-splines as basic functions, to the solution of the 2D half-space acoustic problems with absorbing boundary condition was applied. Fast multipole method was used to accelerate the solution of the BEM. In (Rabisse *et al.*, 2019) a FDM in time domain was applied for simulating the acoustic field in the room with geometrical relief on the room surfaces.

To mitigate drawbacks of the FEM to the solution of acoustic problems, in (Xiangyu *et al.*, 2020) the MLM in the local Galerkin weak form instead of the mesh grid required in the global Galerkin weak form was applied. In (Chen *et al.*, 2017a) the FEM and BEM coupling approach (hybrid method) was used for vibro-acoustic analysis. The FEM and BEM were used to model the structure and acoustic field respectively. Considering the advantages of MLM, this method was part of many hybrid methods. For example, in (Xiangyu *et al.*, 2018) a hybrid MLM – infinite acoustic wave envelope element method (WEEM) was proposed for acoustic radiation prediction. This hybrid method provides results with high accuracy and also has a faster convergence speed than the standard hybrid method FEM-WEEM. In (Wu *et al.*, 2019) the influence of acoustic waves to structural vibrations was solved by a hybrid method consisting of FEM and BEM; it was so called the acoustic-structural coupling problem. In (Shaposhnikov, Jensen, 2018) an interaction between panel vibrations and the acoustic pressure in closed domain was treated. To solve the problem, the FEM and BEM and the numerical Green's function (exact) were applied (hybrid method). For two-dimensional acoustic radiation problems, in (Li *et al.*, 2020) the coupling of the RBF interpolation on triangular mesh with standard FEM was proposed. It was pointed out that coupled methods (hybrid method) had significant superiorities over the standard FEM. In (Pilch, 2019), in Imagine Sources Method (ISM), the procedure of selection of main simulation parameters, i.e. number of rays and ray tracing time, was proposed. A range of input parameters was controlled through criterion between a model and a measurements results.

Four commercial software tools (ART A, Dirac, EASERA, and WinMLS), widely used in room acoustics, were compared in (Alvarez-Morales, *et al.*, 2016). Comparison was drawn up from the room impulse response measured with each tool under the same conditions.

In (Brański, Prędka, 2018) MLM was proposed to solve the acoustic boundary problem with impedance boundary conditions imposed on the boundary of the domain. In the solution in the form of a series, the base functions were the nonsingular RBF. From among many such RBF functions, Hardy's multiquadratic functions (H-RBF) were selected. Because H-RBF was parameterized, with the shape parameter C, a relationship was found between this parameter and the physical parameters of the problem. So, the coefficient C was expressed analytically as a function of the separate quantities, i.e. the absorption coefficient α, acoustic frequency f and the number of influence points n.

Under the above assumption that the C coefficient was found separately for physical parameters, MLM based on H-RBF was efficient at low and middle frequencies.

In the next paper (Prędka, Brański, 2020), assuming the same boundary conditions as before, the MLM to the solution of the acoustic indoor problem in the full range of acoustic frequencies was worked out. First of all three types of RBF were considered, i.e. H-RBF, inverse multiquadratic (I-RBF) and Duchon's (D-RBF).

Next, the relations between physical and approximate solution parameters primarily were shown, but only for the mean value of the relative error in the domain. $\varepsilon_m \leq 5\%$. For this purpose it was shown that the parameter C, only in H-RBF and I-RBF, was not dependent on the absorption coefficient α. However, the C was changed hyperbolically with respect to frequency f and this change was different for separate RBFs. The influence of frequency f on the number of serial elements n was also determined. Hence, the conclusion that for all RBFs, even $n = 15$ provided results with accuracy $\varepsilon_m \leq 5\%$.

Finally it was shown that for all values of acoustic frequencies f and all values of absorption coefficients α, the MLM with tested RBFs ensured the good acoustic field in the sense of mean value accuracy in the domain. But for low frequencies and low absorption coefficients the approximate distribution of the acoustic field was not similar to the exact one. It seems that the natural way to improve results was to tighten the criterion of searching for solution parameters.

In this paper, based on the minimization of the relative error ε_m and similar, based on the error but in the selected point of the domain $\varepsilon(x)$, an efficiency of MLM is analyzed in detail. Quite similar like in (Prędka, Brański, 2020), first the relations between physical parameters and approximate solution parameters are shown. Next, the most effective function RBF is indicated. At the end, for the most effective RBF and fixed n, the distribution of the acoustic field in the domain is calculated, especially at low frequencies and low values of the absorption coefficient.

2. Formulation of the boundary acoustic problem

Let an acoustic boundary problem in the domain Ω with a boundary Γ be given. In steady state this problem is described by Helmholtz equation and acoustic boundary conditions. For example, the cross section of simple acoustic room is considered in which the floor is modelled through the Neumann boundary condition (**N**), but the walls and ceiling are modelled through impedance Robin boundary conditions (**R**); geometry of this problem is in Fig. 1. So, the problem can be finally described by (Prędka, Brański, 2020),

$$\mathcal{L}u(\mathbf{x}) = \Delta u(\mathbf{x}) + k_f^2 u(\mathbf{x}) = f(\mathbf{x}), \quad \mathbf{x} = \mathbf{x}' \in \Omega, \tag{1}$$

$$D_{\mathbf{n}}u(\mathbf{x}) = 0, \qquad \mathbf{x} \in \mathbf{N}, \tag{2}$$

$$D_{\mathbf{n}}u(\mathbf{x}) + z_0 u(\mathbf{x}) = 0, \qquad \mathbf{x} \in \mathbf{R}, \tag{3}$$

where $u(\mathbf{x})$ is the acoustic potential, $f(\mathbf{x})$ – exciting of the acoustic wave, $\mathbf{x} = (x, y, z)$, k_f – wave number, $k_f = \omega_f/c$, $\omega_f = 2\pi f$ – angular exciting frequency, c – speed of sound, $D_{\mathbf{n}}u(\mathbf{x}) = \partial u(\mathbf{x})/\partial \mathbf{n}$, $\mathbf{n}$ – unit normal vector pointing outward, $z_0(\mathbf{x}) = (\omega\rho)/z(\mathbf{x})$, ρ – air density.

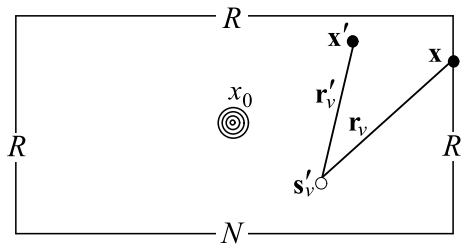

Fig. 1. Geometry of the acoustic problem.

An acoustic source $f(\mathbf{x})$ in 2D is assumed as the 0-order, Hankel function of the second kind, i.e. $f(\mathbf{x}) = AH_0^{(2)}(k_f r)$. The intensity of the source A is chosen, so that the L_m (Eq. (9)) takes the same value for different values of the absorption coefficient α and frequencies f (Brański *et al.*, 2017).

A surface acoustic impedance $z(\mathbf{x})$ is given by (Prędka, Brański, 2020),

$$z(\mathbf{x}) = p(\mathbf{x})/v(\mathbf{x}) = \rho c \frac{1 + (1 - \alpha(\mathbf{x}))^{1/2}}{1 - (1 - \alpha(\mathbf{x}))^{1/2}}, \tag{4}$$

where $p(\mathbf{x}) = i\rho\omega u(\mathbf{x})$ is an acoustics pressure, $v(\mathbf{x}) = -D_{\mathbf{n}}u(\mathbf{x})$ – particle velocity, $i = \sqrt{-1}$, $\alpha(\mathbf{x})$ – material absorption coefficient (Kuttruff, 2000).

3. Approximate solution by MLM via RBF

An approximate solution of the problem is assumed as the series,

$$\widetilde{u}(x') = \sum_{\nu} a_\nu \mathsf{R}(r'_\nu) = |\mathbf{s}_\nu - \mathbf{x}'|, \tag{5}$$

where $\mathbf{s}_\nu \in \overline{\Omega} = \Omega \cup \Gamma$, $\mathbf{x}' \in \Omega$ (Fig. 1).

Three forms of RBF $\mathsf{R}(r'_\nu)$ are considered (Prędka, Brański, 2020): H-RBF, $(\mathsf{R}(C, r'_\nu))$, I-RBF $(\mathsf{R}(C, r'_\nu))$, D-RBF $(R(r'_\nu))$. Note that H-RBF and I-RBF depend on the shape coefficient C, which should be determined.

Now, in the domain $\overline{\Omega}$, the set of collocation points $\{\mathbf{x}_\mu\}$ is selected, where $\mu = 1, 2, ..., m = n$, $\mathbf{x}'_\mu \in \Omega$, $\mathbf{x}_\mu \in \Gamma$ (Fig. 2). Substituting Eq. (5) to Eqs (1)–(3) one has,

$$\sum_{\nu} a_\nu \left(D_x^2 \mathsf{R}(r'_{\nu\mu}) + D_y^2 \mathsf{R}(r'_{\nu\mu}) + k^2 \mathsf{R}(r'_{\nu\mu})\right) = f(\mathbf{x}'_\mu), \tag{6}$$

$$\sum_{\nu} a_\nu D_{\mathbf{n}} \mathsf{R}(r_{\nu\mu}) = 0, \quad \mathbf{x}_\mu \in \mathbf{N}, \tag{7}$$

$$\sum_{\nu} a_\nu \left(D_{\mathbf{n}} \mathsf{R}(r_{\nu\mu}) + z_0(\mathbf{x}_\mu)\mathsf{R}(r_{\nu\mu})\right) = 0, \quad \mathbf{x}_\mu \in \mathbf{R}, \tag{8}$$

where: e.g. $D_x^2(.) = \partial^2(.)/\partial(\mathbf{x}'_\mu)^2$.

4. Optimization, numerical calculations, results

4.1. Acoustic field parameters

To derive a goal function, sound field parameters in the domain are defined. First, an exact acoustic pressure $p(\mathbf{x})$ (Brański *at al.*, 2017) and mean value of the acoustic pressure p_m in the 2D domain Ω are calculated, where $p_m = 1/n_i \sum_i p(\mathbf{x}_i)$, $i = 1, 2, ..., n_i$ is the number of calculated points $\mathbf{x}_i = \mathbf{x}'_i \in \Omega$; they describe acoustic fields in Pa. Next, the value of the sound pressure level $L(\mathbf{x})$ at the point $\mathbf{x} = \mathbf{x}' \in \Omega$ and mean value of the sound pressure level L_m in the domain Ω are given jointly in a compact form; they describe acoustic fields in dB,

$$\{L(\mathbf{x}), L_m\} = \left\{10\log\left(p(\mathbf{x})/p_0\right)^2, 10\log\left(p_m/p_0\right)^2\right\}, \tag{9}$$

where $p_0 = 2 \cdot 10^{-5}$ Pa. Consequently, for approximate pressures $\{\widetilde{p}(\mathbf{x}), \widetilde{p}_m\}$, approximated acoustic pressure levels are obtained respectively,

$$\left\{\widetilde{L}(\mathbf{x}), \widetilde{L}_m\right\} = \left\{10\log\left(\widetilde{p}(\mathbf{x})/p_0\right)^2, 10\log\left(\widetilde{p}_m/p_0\right)^2\right\}. \tag{10}$$

To notice quantitative change, in dB, between exact and approximated acoustic fields at the point and in the domain respectively, the appropriate differences are calculated and they could be presented jointly too, i.e.:

$$\{\delta(\mathbf{x}), \delta_m\} = \left\{\left|L(\mathbf{x}) - \widetilde{L}(\mathbf{x})\right|, \left|L_m - \widetilde{L}_m\right|\right\}. \tag{11}$$

Finally, to notice a quantitative change, in percentage, between the same quantities, one can use the appropriate relative error formulas,

$$\{\varepsilon(\mathbf{x}), \varepsilon_m\} = \{|\delta(\mathbf{x})/L(\mathbf{x})| \cdot 100\%, |\delta_m/L_m| \cdot 100\%\}. \tag{12}$$

Each of these two errors is a goal function and minimizing them leads to finding optimal solutions. Hereunder, first the error in the domain ε_m and then the error at the point $\varepsilon(\mathbf{x})$ are minimized.

The following global values and symbols are assumed: $\rho = 1.205$ kg/m^3, $c = 344$ m/s, $\{a_x, b_x\} = \{0, 5\}$ m, $\{a_y, b_y\} = \{0, 2.5\}$ m. The source is placed at the point $\mathbf{x}_0 = \{x_0, y_0 = \{2.5, 1.25\}$ m. Acoustic values imposed on the boundaries are $z_0(a_x) \equiv z_0(b_x) \equiv z_0(b_y) = Z$ and $z_0(a_y) = 0$. Influence points are marked by "$\circ$" and collocation points are marked by "$\bullet$". Both kinds of points coincide with each other; the rest of the labels are depicted in Fig. 2.

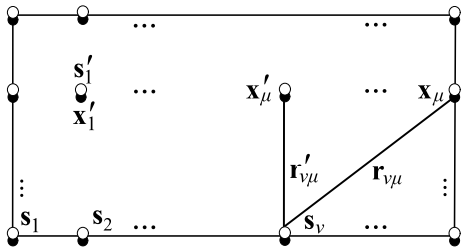

Fig. 2. Distribution of all points in the $\overline{\Omega}$.

Numerical details are presented for selected discrete values of the full scope of the absorption coefficient, i.e. $\{\alpha\} = \{0.1, \text{step}\,0.1, 0.9\}$ and selected acoustic frequencies, represented by octave frequencies, namely $f = 125, 250, ..., 16000\}$ Hz.

4.2. Optimization of the solution to the problem in the domain

In this subsection, minimization of the error ε_m, Eq. (12), leads to the optimal solution of the problem. Hereunder, open marks, regardless of their shapes and colours, apply to $n = 15$ elements in the series, while solid marks apply to $n = 45$ ones. Furthermore, blue, red and green marks, regardless of shape, are refered to H-RBF, I-RBF and D-RBF respectively.

First, the relations between physical parameters and approximate solution parameters are found.

1) At this stage, the parameter C and the error ε_m, as a function (f, n), are jointly presented. The left ordinate axis shows values of $C = C(f, n)$, while the right ordinate axis shows values of $\varepsilon_m(f, n)$. The vertical lines in the figure mean $\varepsilon_d(f, n) = \varepsilon_{\max}(f, n) - \varepsilon_{\min}(f, n)$, where $\varepsilon_{\max}(f, n)$ and $\varepsilon_{\min}(f, n)$ are maximum and minimum error $\varepsilon_m(f, n)$ respectively, and these values are achieved for $\alpha \in \langle 0.1, 0.9\rangle$. All results are presented in Figs 3 and 4.

   Values of $C(f, n)$, for $n = 15$, between $f = 125$ Hz and $f = 1000$ Hz form an almost straight line, hence $C = 5$. But for frequency $f = 500$ Hz and for $n = 15$, the $\varepsilon_d(f, n)$ rapidly increases and for $n = 45$, the $\varepsilon_d(f, n)$ is relatively small. This is the reason for increasing n from $n = 15$ to $n = 45$ for this frequency. For the frequencies greater than $f = 500$ Hz, for $n = 45$, discrete values $C(f, n)$ may be interpolated by a parabolic line in the form $C = a_1 f^2 + a_2$. For H-RBF, $a_1 = -8.7435 \cdot 10^{-9}$, $a_2 = 4.2514$, but for I-RBF, $a_1 = -7.5240 \cdot 10^{-9}$, $a_2 = 4.6861$.

2) At this point, the most effective function RBF is indicated. To achieve this, errors $\varepsilon_m = \varepsilon_m(f, n, \alpha)$ are compared for separate α, for a fixed number n and selected for representative frequency $f = \{250, 1000, 4000\}$ Hz. The RBF which achieves the smallest error $\varepsilon_m(f, n, \alpha)$ is considered as the most effective; results are depicted in figures below.

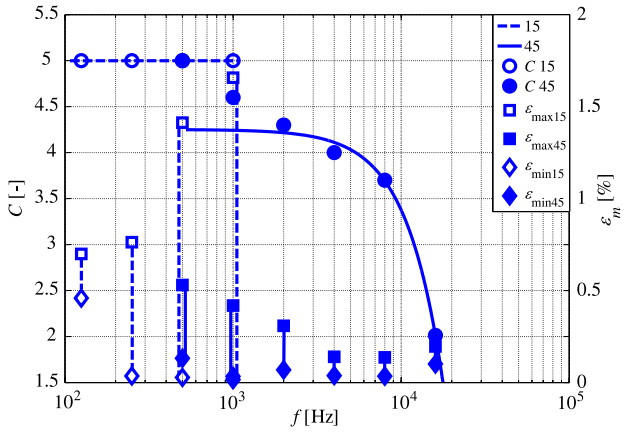

Fig. 3. The parameter $C(f, n)$ (LHS axis) and $\varepsilon_m(f, n)$ (RHS axis) for H-RBF.

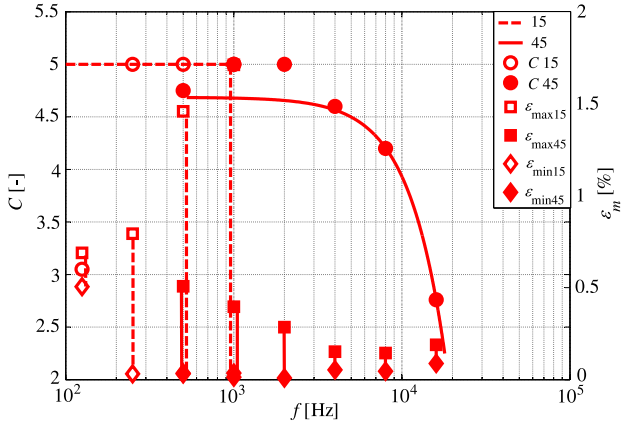

Fig. 4. The parameter $C(f, n)$ (LHS axis) and $\varepsilon_m(f, n)$ (RHS axis) for I-RBF.

Figures 5–7 show that for H-RBF and I-RBF errors ε_m are considerably smaller than for D-RBF and for H-RBF and I-RBF errors are comparable. However, in general the error ε_m is the smallest for H-RBF. Hence, it is considered that MLM with the base H-RBF is the most effective. All the following calculations are made for H-RBF. So the index "H" is omitted in the labels, e.g. $L_H \to L$, $\varepsilon_H(\mathbf{x}) \to \varepsilon(\mathbf{x})$, $\varepsilon_{m;H;O} \to \varepsilon_{m;O}$ and so on.

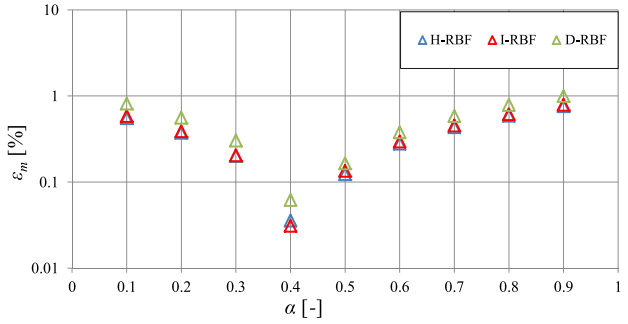

Fig. 5. Errors $\varepsilon_m(f, n, \alpha) = \varepsilon_m(250, 15, \alpha)$ for separate RBF.

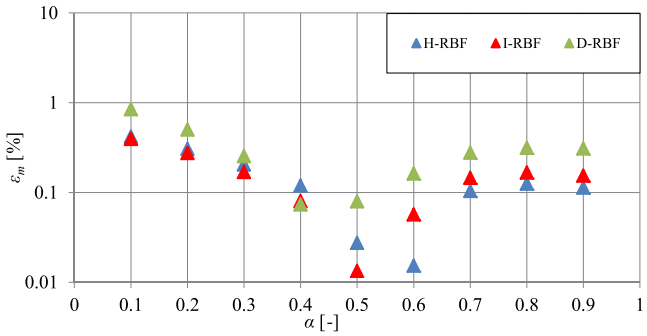

Fig. 6.Errors $\varepsilon_m(f,n,\alpha) = \varepsilon_m(1000,45,\alpha)$ for separate RBF.

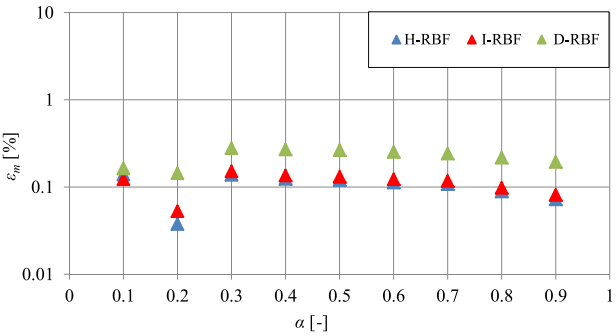

Fig. 7. Errors $\varepsilon_m(f,n,\alpha) = \varepsilon_m(4000,45,\alpha)$ for separate RBF.

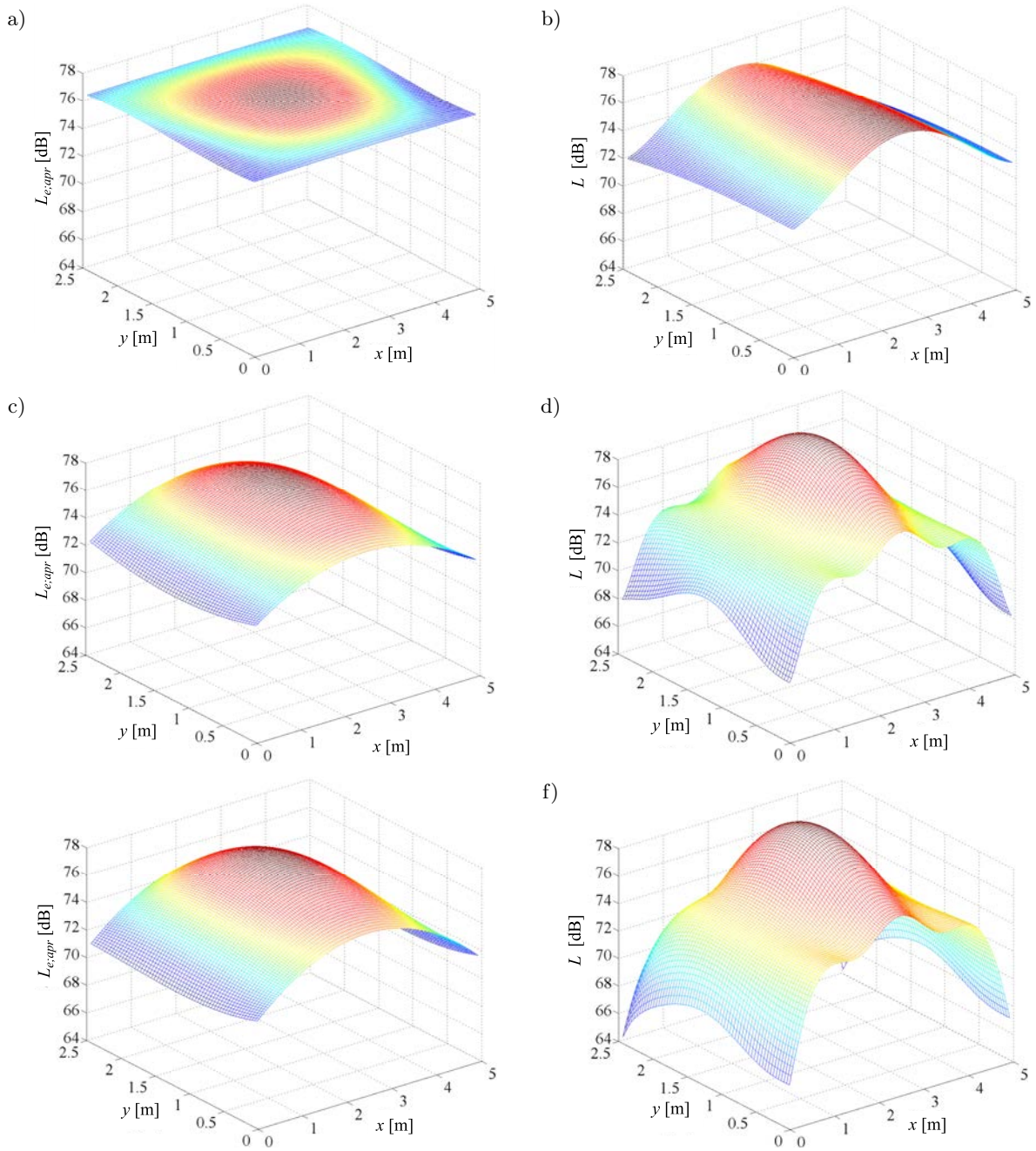

Fig. 8. LHS – $L_{e;apr} = L_{e;apr}(\mathbf{x})$, RHS – $L = \widetilde{L}(\mathbf{x})$: a) and b) $f = 250$ Hz, c) and d) $f = 1000$ Hz, e) and f) $f = 4000$ Hz.

Table 1. Comparison of the optimal errors values in the domain and at the point.

f [Hz]	$\delta_{\ldots}(\mathbf{x}_w)$ [dB]	$\varepsilon_{\ldots}(\mathbf{x}_w)$ [%]	$\delta_{\ldots}/\delta^w_{\ldots}$ [dB]	$\varepsilon_{\ldots}/\varepsilon^w_{\ldots}$ [%]
250	$\delta = 3.0007$	$\varepsilon = 3.9351$	$\delta_m = 0.4146$	$\varepsilon_m = 0.5552$
	$\delta_O = 0.0217$	$\varepsilon_O = 0.0284$	$\delta^w_{m;O} = 3.4576$	$\varepsilon^w_{m;O} = 4.6101$
1000	$\delta = 2.6990$	$\varepsilon = 3.7092$	$\delta_m = 0.3142$	$\varepsilon_m = 0.4186$
	$\delta_O = 0.7219$	$\varepsilon_O = 0.9971$	$\delta^w_{m;O} = 0.4725$	$\varepsilon^w_{m;O} = 0.6301$
4000	$\delta = 2.1097$	$\varepsilon = 2.9205$	$\delta_m = 0.1049$	$\varepsilon_m = 0.1399$
	$\delta_O = 1.1191$	$\varepsilon_O = 1.5510$	$\delta^w_{m;O} = 0.1166$	$\varepsilon^w_{m;O} = 0.1555$

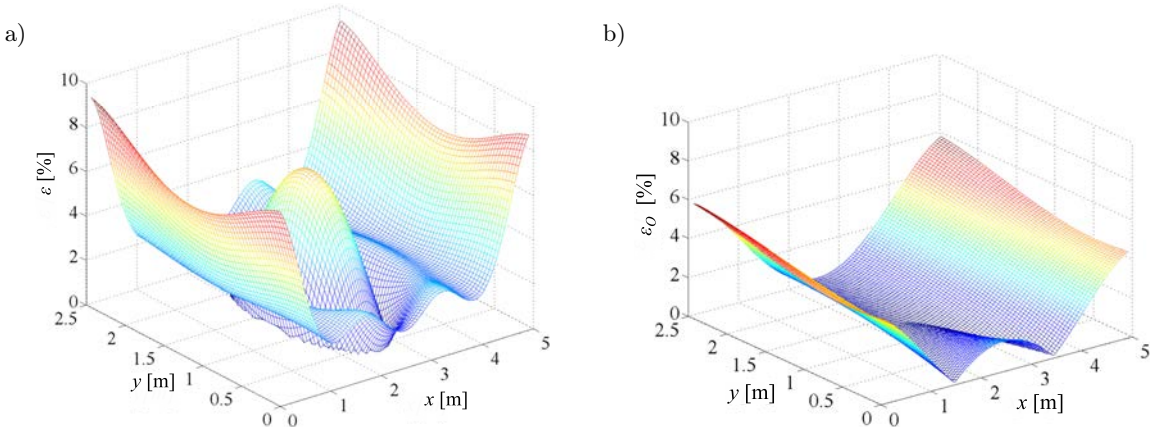

Fig. 9. LHS – $\varepsilon = \varepsilon(\mathbf{x})$, RHS – $\varepsilon_O = \varepsilon_O(\mathbf{x})$.

3) Now, the effect of minimizing the error ε_m is presented. First, for the most effective H-RBF and chosen $f = \{250, 1000, 4000\}$ Hz, $\alpha = 0.1$, the distribution of the exact $L_e(\mathbf{x})$ and approximate $\widetilde{L}(\mathbf{x})$ acoustic fields are calculated. An exact solution $L_e(\mathbf{x})$ is replaced by its mean square approximation $L_{e;apr}(\mathbf{x})$; results are depicted in Fig. 8.
4) To show the effect of minimizing the error ε_m, two acoustic fields in the domain are compared only for $f = 250$ Hz; for remaining frequencies, main results are in the Table 1. Firstly, it is calculated for the parameters obtained in (Prędka, Brański, 2020), i.e. $n = 45$ and $C = 2.205$. For these parameters $\widetilde{L}(\mathbf{x}) = L(\mathbf{x})$ is calculated, it is the solution for H-RBF and error $\varepsilon_m < 5\%$. The error of this solution $\varepsilon_m(x)$ is calculated according to Eq. (12), where $L(\mathbf{x}) = L_{e;apr}(\mathbf{x})$; results are presented in Fig. 9 (LHS); the value of the error is $\varepsilon_m = 3.2377\%$.

Secondly, sound field is calculated for the minimum error $\varepsilon_m = \varepsilon_{m;\min}$, i.e $\varepsilon_{m;O}$, now $n = 15$ and $C = 5$. For this data, $\widetilde{L}(\mathbf{x}) = L_O(\mathbf{x})$ is calculated, i.e. the solution for H-RBF and optimal n and C. In this case, the error $\varepsilon_O(x)$ is calculated analogously as above; results are in Fig. 9 (RHS). The value of the error is $\varepsilon_{m;\min} = \varepsilon_{m;O} = 2.1020\%$.

The comparison of $\varepsilon(x)$ and $\varepsilon_O(x)$ shows, at first glance, that optimization of parameters of H-RBF solution ensures expected better results. In addition, the average values ε_m and $\varepsilon_{m;o}$ $\varepsilon_{m;O}$ quantitatively confirm this conclusion, see Table 1.

In the next subsection, the idea of H-RBF solution optimization is developed based on minimizing the error at the point of the domain.

4.3. Optimization of the solution to the problem at the point

To minimize the error $\varepsilon(\mathbf{x}_w)$, the point $\mathbf{x}_w = (x_w, y_w) = (0.2400, 0.1587)$ is chosen. At this point, for $f = 250$ Hz, the difference $\delta_H(\mathbf{x}_w) = 3$ dB, Eq. (11), and the error $\varepsilon(\mathbf{x}_w) = 3.9351\%$, Eq. (12), where $L(\mathbf{x}_w) = L_{e;apr}(\mathbf{x}_w)$ and $\widetilde{L}(\mathbf{x}_w) = L(\mathbf{x}_w)$. The error minimization $\varepsilon(\mathbf{x}_w)$ is carried out in the same way as the error ε_m.

Because H-RBF contains the shape parameter C, its effect on $\varepsilon(x_w)$ is determined; results are shown in Fig. 10. Hence, for $C = 0.011$, the error $\varepsilon(x_w)$ has a minimum value of $\varepsilon_{\min}(\mathbf{x}_w) = \varepsilon_O(\mathbf{x}_w) = 0.0284\%$, while $\delta_{\min}(\mathbf{x}_w) = \delta_O(\mathbf{x}_w) = 0.0217$ dB.

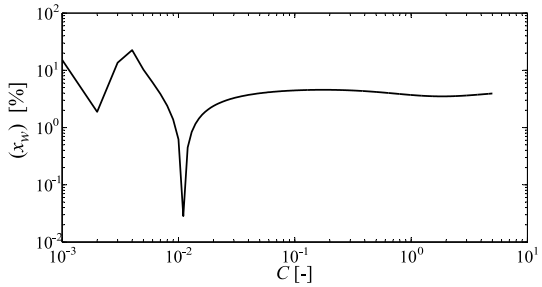

Fig. 10. Error $\varepsilon(\mathbf{x}_w)$ in the function of the C shape parameter.

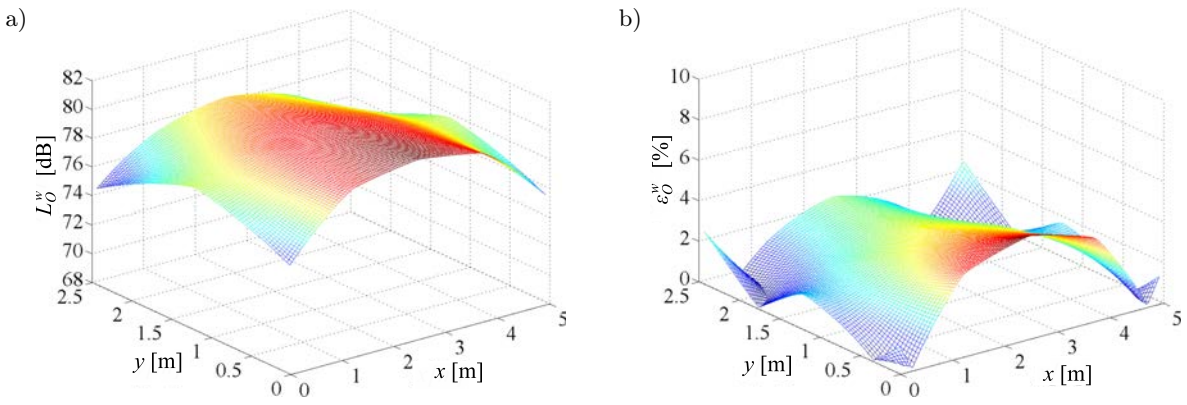

Fig. 11. Optimization of the solution at the point $\mathbf{x}_w$; LHS – $L_O^w(\mathbf{x})$, RHS – $\varepsilon_O^w(\mathbf{x})\varepsilon_o^w(\mathbf{x})$.

For this value C, the acoustic field $\widetilde{L}(\mathbf{x}) = L_O^w(\mathbf{x})$ and the error $\varepsilon_O^w(\mathbf{x})$ are calculated, see Fig. 11. Next, the appropriate mean values are calculated, namely: the difference $\delta_{m;O}^w = 1.6616$ dB and the mean error value $\varepsilon_{m;O}^w = 2.1637\%$. Both of these values should be related to $\delta_{m;O} = 1.3796$ dB and $\varepsilon_{m;O} = 1.7964\%$, respectively.

From the analysis of the optimization of the solution at the point it follows that very good results can be achieved, but only at this point. This happens at the cost of worsening the solution in other parts of the domain, which can be measured by either the mean value of the difference $\delta_{m;O}^w$ in dB or/and the mean value of the error $\varepsilon_{m;O}^w$ in %.

5. Conclusions

In the paper, two aspects of optimization were proposed to improve an efficiency of MLM. Firstly, it was done by minimizing the average error ε_m in the domain Ω and secondly, by minimizing the error $\varepsilon(\mathbf{x}_w)$ at the point $\mathbf{x}_w \in \Omega$.

First of all, for H-, I- and D-RBF respectively, the number of elements n in the series was established. It was found that in the case of H- and I-RBF, parameter C has a large influence on the number of elements n in the series as a function of frequency f. This relation, $C = C(f, n)$, was found in an analytical form, but alternatively for low and medium and high frequencies.

Further, the most effective base function RBF was pointed out. For this RBF, i.e. H-RBF, the optimization of parameters of the solution was performed. For this purpose, the error ε_m was minimized, so $\varepsilon_m = \varepsilon_{m;\min}$. To show the effect of minimizing, the error $\varepsilon_{m;\min}$ was compared with the error ε_m, i.e. for the solution with parameters without optimization. Then both solutions were presented.

At the end, for H-RBF the optimization of parameters of the solution were performed, minimizing the error at the point $\varepsilon(\mathbf{x}_w)$, hence $\varepsilon(\mathbf{x}_w) = \varepsilon_{\min}(\mathbf{x}_w)$ was obtained. The effect was compared to the one of minimizing the mean error in the domain ε_m. In this case, better results were obtained only at this point. From analysis of the problem arise the following conclusions:

1) From the engineering point of view, the optimal number of elements n is $n = 15$ for lower frequencies and $n = 45$ for medium and higher frequencies.
2) For low frequencies, between $f = 125$ Hz and $f = 500$ Hz, and for $n = 15$, the shape parameter $C(f, n)$ is presented in the form of almost straight line, hence $C = C(f, n) = C(f, 15) = 5$. In the remaining range of acoustic frequencies and $n = 45$, a function graph $C = C(f, n) = C(f, 45)$ is interpolated by a parabolic line.
3) H-RBF provides the best results out of three tested base functions.
4) Optimization parameters of the H-RBF solution, based on minimizing the average error in the domain, improves the solution in measure of this error.
5) Optimization parameters of the H-RBF solution, based on minimizing the error at one point of the domain, improves the solution only in this point.

References

1. Álvarez-Morales L., Galindo M., Girón S., Zamarreño T., Cibrián R.M. (2016), Acoustic characterization by using different room acoustics software tools: A comparative study, *Acta Acustica united with Acustica*, **102**(3): 578–591, doi: 10.3813/AAA.918975
2. Brański A., Kocan-Krawczyk A., Prędka E. (2017), An influence of the wall acoustic impedance on the room acoustics. The exact solution, *Archives of Acoustics*, **42**(4): 677–687, doi: 10.1515/aoa-2017-0070.
3. Brański A., Prędka E. (2018), Nonsingular meshless method in an acoustic indoor problem, *Archives of Acoustics*, **43**(1): 75–82, doi: 10.24425/118082.
4. Chen L., Marburg S., Zhao W., Liu C., Chen H. (2019), Implementation of isogeometric fast multipole boundary element methods for 2D half-space acoustic

scattering problems with absorbing boundary condition, *Journal of Theoretical and Computational Acoustics*, **27**(2): 1850024, doi: 10.1142/S259172851850024X.

5. Chen L., Zhao W., Liu C., Chen H. (2017a), 2D structural acoustic analysis using the FEM/FMBEM with different coupled element types, *Archives of Acoustics*, **42**(1): 37–48, doi: 10.1142/S259172851850024X.
6. Kuttruff H. (2000), *Fundamentals of Physical Acoustics, Room Acoustic*, Wiley–Interscience, New York.
7. Li W., Zhang Q., Gui Q., Chai Y. (2020), A Coupled FE-Meshfree Triangular Element for Acoustic Radiation Problems, *International Journal of Computational Methods*, doi: 10.1142/S0219876220410029.
8. Meissner M. (2019), Prediction of low-frequency sound field in rooms with complex valued boundary conditions on walls, *Vibrations in Physical Systems*, **30**(1): 2019127.
9. Meissner M., Wiśniewski K. (2019), Influence of room modes on low-frequency transients: Theoretical modeling and numerical predictions, *Journal of Sound and Vibration*, **448**: 19–33, doi: 10.1016/j.jsv.2019.02.012.
10. Pilch A. (2019), *Optimization based validation of room acoustic models*, AGH University of Science and Technology, Kraków, Poland.
11. Prędka E., Brański A. (2020), Analysis of the room acoustic with impedance boundary conditions in the full range of acoustic frequencies, *Archives of Acoustics*, **45**(1): 85–92, doi: 10.24425/aoa.2020.132484.
12. Rabisse K., Ducourneau J., Faiz A., Trompette N. (2019), Numerical modelling of sound propagation in rooms bounded by walls with rectangular-shaped irregularities and frequency-dependent impedance, *Journal of Sound and Vibration*, **440**: 291–314, doi: 10.1016/j.jsv.2018.08.059.
13. Shaposhnikov K., Jensen M.J.H. (2018), Panel contribution analysis based on FEM, BEM and numerical Green's function approaches, *Journal of Theoretical and Computational Acoustics*, **26**(3): 1850037, doi: 10.1142/S2591728518500378.
14. Shi S., Liu K., Xiao B., Jin G., Liu Z. (2019), Forced acoustic analysis and energy distribution for a theoretical model of coupled rooms with a transparent opening, *Journal of Sound and Vibration*, **462**: 114948, doi: 10.1016/j.jsv.2019.114948.
15. Van Horssen W.T., Wang Y., Cao G. (2018), On solving wave equations on fixed bounded intervals involving Robin boundary conditions with time-dependent coefficients, *Journal of Sound and Vibration*, **424**: 263–271, doi: 10.1016/j.jsv.2018.03.009.
16. Wu H., Yu L., Jiang W. (2019), A coupling FEM/BEM method with linear continuous elements for acoustic-structural interaction problems, *Applied Acoustics*, **150**: 44–54, doi: 10.1016/j.apacoust.2019.02.001.
17. Xiangyu W., Yang X., Jiachi Y. (2018), A meshfree radial point interpolation coupled with infinite acoustic wave envelope element method for computing acoustic fields, *Acta Acustica united with Acustica*, **104**(1): 64–78, doi: 10.3813/AAA.919146.
18. Xiangyu Y., Wei L., Yingbin C. (2020), A truly meshfree method for solving acoustic problems using local weak form and radial basis functions, *Applied Mathematics and Computation*, **365**: 124694, doi: 10.1016/j.amc.2019.124694.